

[Co_xCu_{1-x}(DDOP)(OH₂)(NO₃)](NO₃): hydrogen bond-driven distortion of cobalt(II) by solid solution ‘network mismatch’†John Fielden,^{a,c} De-Liang Long,^a Manfred Speldrich,^b Paul Kögerler^{*b,c} and Leroy Cronin^{*a}

Received 22nd January 2012, Accepted 8th February 2012

DOI: 10.1039/c2dt11055e

Late-first row transition metal nitrate complexes of the tetradentate N-donor ligand *cis*-3,5-bis[(2-pyridinyleneamino)-*trans*-hydroxycyclohexane (DDOP) adopt a mono-cationic [M(DDOP)(H₂O)(NO₃)]⁺ structure (M = Co, **1**; Cu, **2**; Zn, **3**) in which the DDOP ligand occupies the equatorial plane. The complexes are essentially isostructural and isomorphous, allowing the Co(II) and Cu(II) complexes to co-crystallize in mixed-metal solid solutions with the formula [Co_xCu_{1-x}(DDOP)(NO₃)(H₂O)](NO₃), where *x* = 0.4 (**4**), 0.1 (**5**), and 0.7 (**6**). For **4**, structural and magnetochemical analysis indicate that the geometry of the octahedral Co(II) complex distorts to match that of the dominant Jahn–Teller distorted Cu(II) center. Magnetic susceptibility data of octahedral Co(II) are sensitive to ligand geometry distortions and have been analyzed accordingly, comparing **4** to the reference systems **1** and **2**. Bond valence calculations have been used to estimate the relative stabilities of the six hydrogen bonded networks, suggesting that the stretching of the Co(II) coordination sphere in **4** is assisted by adoption of the most stable hydrogen bonded network; but that in **6** this is overcome by a higher loading of Co. This family of complexes therefore represent predictable metal-based tectons which can help probe the influence of secondary non-covalent interactions over metal coordination geometries and properties.

Introduction

Understanding the formation of solids based on molecular building blocks is vital to the goal of engineering materials with useful macroscopic physical properties.¹ While the importance of hydrogen bonding in the self-assembly of molecular solids is well known, its contribution is often difficult to delineate from those of other intermolecular interactions. Weaker non-covalent interactions² and entropic factors³ can govern selection between competing hydrogen bonded networks of similar energies, and hydrogen bonds can in turn influence metal–ligand bonds.⁴ Hydrogen bonds also directly affect solid state properties, for example by providing magnetic exchange pathways.^{5,6} Although the interplay of supramolecular interactions is increasingly appreciated, the structural complexity and unpredictability of coordination compounds makes controlled testing of their effects on structure and properties difficult. For this reason, the

relationships between hydrogen bonding and metal coordination are only starting to be understood.

Co-crystallization of isostructural coordination compounds with isomorphous hydrogen bonded networks provides an opportunity to study these relationships. If there is a significant mismatch between the “natural” coordinate bond lengths of the two metals, co-crystallization may force distortion of one or both metal centers to allow formation of the most stable network: this is likely to be a solid-solution with a disordered distribution of the two metals in crystallographically indistinguishable coordination geometries. Alternatively, the natural coordination geometries may be preserved, potentially resulting in separation of two compounds, formation of an ordered hetero-bimetallic crystal, or formation of a crystal where disorder is apparent in the lengths of the metal–ligand bonds. This tests the relative abilities of the preferred network and coordination geometry to determine the overall structure, and is well-suited to the study of isomorphous structures that are formed by both Jahn–Teller distorted Cu^{II} and more ideally octahedral divalent TM cations. Despite the publication of several isomorphous series of transition metal containing hydrogen bonded networks,^{4f,5b,7} we are unaware of such a study.

The *cis*-3,5-diamino-*trans*-hydroxycyclohexane (*cis,trans*-DAHC)-based family of ligands have provided a useful platform for investigating the roles of metal coordination, hydrogen bonding, hydrophobic and argentophilic interactions in the self-assembly of supramolecular architectures.^{4g,h,8,9} Herein, we present a series of complexes based on the bis-bidentate

^aDepartment of Chemistry, University of Glasgow, G12 8QQ, United Kingdom. E-mail: l.cronin@chem.gla.ac.uk

^bInstitut für Anorganische Chemie, RWTH Aachen University, D-52074 Aachen, Germany. E-mail: Paul.Koegerler@ac.rwth-aachen.de

^cPeter Grünberg Institute – PGI-6, Research Centre Jülich, D-52425 Jülich, Germany. E-mail: p.koegerler@fz-juelich.de

†Electronic supplementary information (ESI) available: discussion of additional mixed-metal structures, estimation of minimum Co(II) coordination sphere distortion. CCDC reference numbers 828952–828955. For ESI and crystallographic data in CIF or other electronic format see DOI: 10.1039/c2dt11055e

imine derivative, *cis*-3,5-bis[(2-pyridinyleneamino)-*trans*-hydroxycyclohexane (DDOP), all isolated as [M(DDOP)(OH₂)(NO₃)](NO₃) salts (M = Co^{II}, Cu^{II}, Zn^{II}) comprising essentially isomorphous hydrogen bonded networks. Co-crystallization of the more regular *pseudo*-octahedral Co^{II} and Jahn–Teller distorted Cu^{II} complexes has allowed use of a combination of crystallography, magnetic measurements and bond valence calculations to study the effects on the coordination geometry and hydrogen bonded network.

Experimental

Materials, methods and instrumentation

The ligand *cis*-3,5-bis[(2-pyridinyleneamino)-*trans*-hydroxycyclohexane (DDOP) was synthesized from *cis*-3,5-diamino-*trans*-hydroxycyclohexane,^{8a} and compound **3** was prepared as previously described.^{4h} All other reagents and solvents were bought as AR grade (Aldrich/Alfa Aesar) and used without further purification. Complexations were performed in ambient atmosphere. IR spectra were measured with a Jasco FTIR-410 spectrometer. Copper and cobalt analyses used ICP-OES (Zentralabteilung für Chemische Analysen, Forschungszentrum Jülich, Germany).

Synthesis of [Co(DDOP)(H₂O)(NO₃)](NO₃) (**1**)

DDOP (0.070 g, 0.226 mmol) in methanol (25 mL) was added dropwise over 3.5 hours to a solution of Co(NO₃)₂·6H₂O (0.0831 g, 0.227 mmol) in methanol (1 mL). A color change from pink to yellow was observed. The solution was stirred for a further 30 minutes, and the volume reduced to *ca.* 3 mL *in vacuo*. After 24 hours, crystallization by diffusion of Et₂O produced **1** as orange crystals (0.029 g, 0.0569 mmol, 25%). FTIR (KBr pellet), ν cm⁻¹: 3385 s (OH), 2940 w (CH), 1638 m (C=N), 1598 s, 1445 s, 1384 s (NO₃⁻), 1299 s (coordinated NO₃⁻), 1071 m (C–O), 783 m. Elemental analysis for C₁₈H₂₂CoN₆O₈, found (calcd): C 42.48 (42.45), H 4.34 (4.35), N 16.27 (16.50)%.

Synthesis of [Cu(DDOP)(H₂O)(NO₃)](NO₃) (**2**)

Addition of Cu(NO₃)₂·3H₂O (0.0548 g, 0.227 mmol) in methanol (5 mL) to a solution of DDOP (0.070 g, 0.226 mmol) in methanol (20 mL) resulted in a color change from blue to bright green. The solution was stirred at room temperature for several hours before the volume was reduced to *ca.* 3 mL *in vacuo*. After 24 hours dark green crystals of **2** (0.060 g, 0.117 mmol, 52%) were produced by diffusion of Et₂O. FTIR (KBr pellet), ν cm⁻¹: 3415 s (OH), 2922 w (CH), 1641 m (C=N), 1603 m, 1385 (NO₃⁻), 1329 s (coordinated NO₃⁻), 1068 m (C–O), 781 m. Elemental analysis for C₁₈H₂₂CuN₆O₈, found (calcd): C 41.95 (42.07), H 4.24 (4.31), N 16.45 (16.35)%.

Synthesis of Co–Cu solid solutions (**4**–**6**)

These were synthesized in a similar fashion to **2**, adding a total of 1 equivalent of Co(NO₃)₂·6H₂O and Cu(NO₃)₂·6H₂O to methanolic solutions of DDOP; in Co : Cu ratios of 1 : 1 (**4**),

1 : 3 (**5**) and 3 : 1 (**6**). Crystals were produced by diffusion of Et₂O into the concentrated solutions.

[Co_{0.4}Cu_{0.6}(DDOP)(H₂O)(NO₃)](NO₃) (**4**)

Dark brown crystals, 58% yield. FTIR (KBr pellet), ν cm⁻¹: 3373 s (OH), 2921 s (CH), 1643 m (C=N), 1601 s, 1385 vs. (NO₃⁻), 1331 vs. (coordinated NO₃⁻), 1070 w (C–O), 827 w, 782 m. Elemental analysis for C₁₈H₂₂Co_{0.4}Cu_{0.6}N₆O₈, found (calcd): C 42.12 (42.23), H 4.27 (4.33), N 16.13 (16.43), Co 4.32 (4.60), Cu 7.45 (7.48)%.

[Co_{0.1}Cu_{0.9}(DDOP)(H₂O)(NO₃)](NO₃) (**5**)

Dark green crystals, 50% yield. FTIR (KBr pellet), ν cm⁻¹: 3382 s (OH), 2922 (m) (CH), 1642 s (C=N), 1601 s, 1385 vs. (NO₃⁻), 1330 vs. (coordinated NO₃⁻), 1070 m (C–O), 828 m, 782 m. Elemental analysis for C₁₈H₂₂Co_{0.1}Cu_{0.9}N₆O₈, found (calcd): Co 1.11 (1.14), Cu 11.1 (11.1)%.

[Co_{0.7}Cu_{0.3}(DDOP)(H₂O)(NO₃)](NO₃) (**6**)

Dark brown crystals, 74% yield. FTIR (KBr pellet), ν cm⁻¹: 3362 s (OH), 2941 (m) (CH), 1643 s (C=N), 1599 s, 1384 vs. (NO₃⁻), 1330 vs. (coordinated NO₃⁻), 1071 m (C–O), 827 m, 782 m. Elemental analysis for C₁₈H₂₂Co_{0.7}Cu_{0.3}N₆O₈, found (calcd): Co 7.97 (8.08), Cu 3.62 (3.73)%.

Magnetochemical analysis

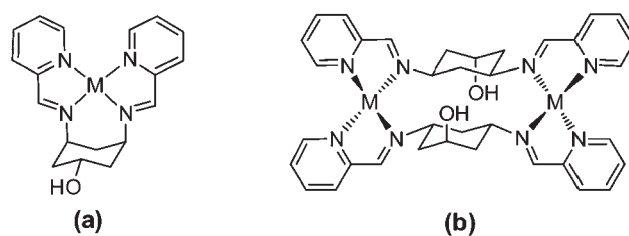
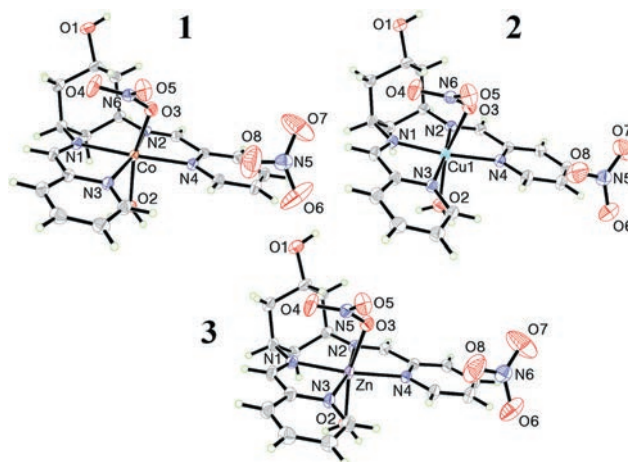
Susceptibility data were recorded using a Quantum Design MPMS-5XL SQUID magnetometer in the temperature range 2–300 K and for fields ranging from 0.1 to 5.0 Tesla. The data were corrected for sample holder and diamagnetic contributions (calculated from tabulated Pascal constants). Modeling and computational analysis were performed using CONDON 2.0.¹⁰

Single-crystal structure determination

Single crystals of **1**–**6** were mounted on the end of a thin glass fiber using Fomblin oil. X-ray diffraction intensity data were measured at 150 K on Nonius Kappa-CCD or Bruker Apex-II CCD diffractometers [λ (Mo-K α) = 0.7107 Å, graphite monochromator]. Structure solution and refinement was carried out with SHELXS-97¹¹ and SHELXL-97¹² *via* WinGX¹³ or SHELXTL.¹⁴ Corrections for incident and diffracted beam absorption effects were applied using empirical methods.¹⁵ All six compounds crystallized in the space group *P*2₁/*c* (**3** was originally solved in *P*2₁/*n*^{4h} but has been transformed to *P*2₁/*c* to aid comparison). The structures were solved by a combination of direct methods and difference Fourier syntheses and refined against $|F|^2$ by the full-matrix least-squares technique. All non-H atoms were refined anisotropically. Hydrogen atoms attached to carbon atoms were included in calculated positions, but those bonded to oxygen atoms were found by difference Fourier techniques and refined isotropically, with O–H distances fixed at *ca.* 0.95 Å to better approximate the position of the proton, rather than electron density, for calculations on the hydrogen bonded

Table 1 Crystallographic data and refinement statistics for compounds 1–6

	1	2	3	4	5	6
Empirical formula	$C_{18}H_{22}CoN_6O_8$	$C_{18}H_{22}CuN_6O_8$	$C_{18}H_{22}ZnN_6O_8$	$C_{18}H_{22}Co_4Cu_6N_6O_8$	$C_{18}H_{22}Co_{0.1}Cu_{0.9}N_6O_8$	$C_{18}H_{22}Co_{0.7}Cu_{0.3}N_6O_8$
$F_w/g\ mol^{-1}$	509.35	513.97	515.81	512.12	513.49	510.73
Cryst. system	Monoclinic	Monoclinic	Monoclinic	Monoclinic	Monoclinic	Monoclinic
$a/\text{\AA}$	9.9345(1)	10.0362(3)	9.9335(3)	10.0170(2)	10.0170(8)	9.963(2)
$b/\text{\AA}$	7.2398(1)	7.3893(2)	7.3304(2)	7.3572(1)	7.3635(6)	7.304(2)
$c/\text{\AA}$	30.0756(5)	29.2108(6)	29.8838(9)	29.4159(7)	29.506(2)	30.128(7)
$\beta/^\circ$	108.139(1)	109.246(2)	108.133(2)	109.0450(1)	110.759(1)	110.317(4)
Space group	$P2_1/c$	$P2_1/c$	$P2_1/c$	$P2_1/c$	$P2_1/c$	$P2_1/c$
$V/\text{\AA}^3$	2055.65(5)	2045.22(9)	2068.0(1)	2049.20(7)	2037.1(3)	2056.0(8)
Z	4	4	4	4	4	4
$\rho_{\text{calcd}}/g\ cm^{-3}$	1.646	1.669	1.657	1.660	1.674	1.650
μ/mm^{-1}	0.897	1.130	1.249	1.030	1.112	0.965
T/K	150(2)	150(2)	150(2)	150(2)	150(2)	150(2)
No. observations (unique)	15 414 (4593)	19 463 (4622)	15 290 (4654)	16 129 (4032)	23 743 (4223)	23 727 (4279)
R_{int}	0.0429	0.0432	0.0392	0.0328	0.0520	0.0964
Residuals: $R; R_w$	0.0381; 0.0951	0.0314; 0.0813	0.0406; 0.0936	0.0346; 0.0812	0.0339; 0.0810	0.0623; 0.1661

**Scheme 1** Coordination modes of DDOP: (a) mononucleating with octahedral or square-planar metal coordination modes; (b) dinucleating with a tetrahedral metal center.**Fig. 1** Crystal structures of compounds 1 to 3. ADP ellipsoids are drawn at 50% probability level. C atoms are grey; N, blue; O, red; Co, brown; Cu, cyan; Zn, purple. H atoms are white spheres of arbitrary radius.

networks.¹⁶ Crystal data, data collection parameters and refinement statistics are listed in Table 1.

Results and discussion

Synthesis and structures of monometallic compounds 1–3

DDOP offers mono- or dinucleating coordination modes (Scheme 1), but favors mononuclear complexes for Co, Cu and Zn as they have easily accessible *pseudo*-octahedral coordination geometries.⁹ Crystalline samples of 1 to 3 were prepared by reacting the ligand and metal salt at room temperature in methanol, and crystallizing by slow diffusion of diethyl ether (yields *ca.* 20 to 50%). Total yields are likely to be much higher, as NMR studies with Zn^{2+} and Cd^{2+} salts indicate exclusive formation of mononuclear complexes of the type shown in Scheme 1.⁹

The complexes have a *pseudo*-octahedral metal center equatorially chelated by the DDOP N_4 donor set, with axial coordination sites occupied by the coordinating nitrate anion and an aqua ligand located on the opposite side of the metal center to the DDOP alcohol group (Fig. 1). Coordinate bond lengths and angles are summarized in Table 2. Complexes 1 to 3 are isostructural, all showing distortion from idealized octahedral geometry through in their $N_{Py}-M-N_{Py}$ and $O-M-O$ angles. However,

Table 2 Coordinate bond lengths ($R/\text{\AA}$) and angles ($\phi/^\circ$) in the $[\text{M}(\text{DDOP})(\text{H}_2\text{O})(\text{NO}_3)]^+$ complex cations in **1–6**

Complex (M)	Mean equatorial $R_{\text{M-N}}$		ϕ $\text{N}_{\text{py}}\text{-M-N}_{\text{py}}$	Axial $R_{\text{M-O}}$		ϕ O-M-O
	M-N _{Im}	M-N _{Py}		M-OH ₂	M-O ₃ N	
1 (Co)	2.103(2)	2.141(2)	113.33(7)	2.138(2)	2.152(2)	163.05(7)
2 (Cu)	2.004(2)	2.058(2)	105.84(7)	2.364(2)	2.515(2)	162.91(7)
3 (Zn)	2.123(2)	2.132(2)	113.75(8)	2.137(2)	2.280(2)	164.70(7)
4 (Co _{0.4} Cu _{0.6})	2.031(2)	2.079(2)	107.65(8)	2.304(2)	2.433(2)	162.89(7)
Calcd. (Co _{0.4} Cu _{0.6}) ^a	2.044	2.091	108.84	2.274	2.370	162.97
5 (Co _{0.1} Cu _{0.9})	2.005(2)	2.057(2)	106.03(7)	2.353(2)	2.500(2)	162.96(7)
Calcd. (Co _{0.1} Cu _{0.9}) ^a	2.014	2.066	106.59	2.341	2.479	162.92
6 (Co _{0.7} Cu _{0.3})	2.073(3)	2.115(3)	111.3(1)	2.182(4)	2.249(3)	162.9(1)
Calcd. (Co _{0.7} Cu _{0.3}) ^a	2.073	2.116	111.08	2.206	2.261	163.00

^a Predicted coordination sphere for **4** to **6** based on a weighted average of **1** and **2**.

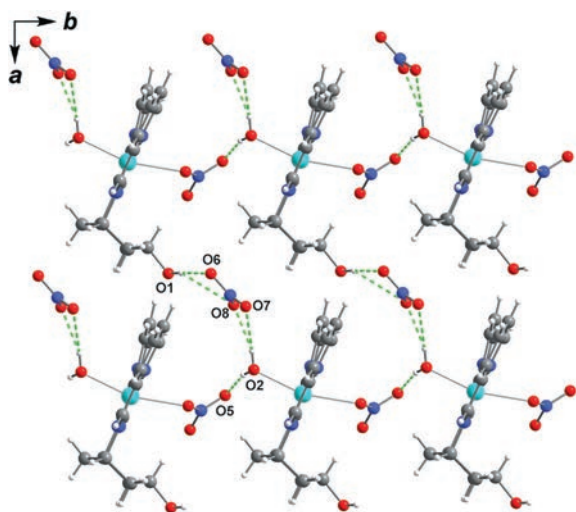


Fig. 2 Section of a hydrogen-bonded layer in $[\text{Cu}(\text{DDOP})(\text{NO}_3)(\text{H}_2\text{O})](\text{NO}_3)$ (**2**), viewed along the crystallographic c axis. Color scheme as Fig. 1, with hydrogen bonds drawn as green dashed lines. The networks of **1** to **4** all show the same basic connectivity.

bond lengths to the axial ligands vary significantly. Axial elongation is insignificant in cobalt(II) complex **1**, while Zn^{II} complex **3** has an elongated Zn–O₃N distance. More dramatic distortion is seen in the Cu^{II} complex **2**, in which the Jahn–Teller effect markedly elongates the axial bonds (up to 0.36 Å) and contracts the equatorial bonds (nearly 0.1 Å) compared to Co^{II} in **1**.

The $[\text{M}(\text{DDOP})(\text{H}_2\text{O})(\text{NO}_3)]^+$ complex cation can be seen as a supramolecular tecton able to donate two hydrogen bonds from one side *via* the aqua-ligand, and another in the opposite direction through the DDOP alcohol group. Consequently, the metal (II) nitrate complexes **1** to **3** form isomorphous 2-dimensional hydrogen bonded networks which run in layers parallel to the crystallographic ab plane (Fig. 2, Table 3). In these networks, hydrogen bonds between the nitrate (O5) and aqua (O2) ligands create chains of cations, which link to each other through further hydrogen bonds between the aqua ligand, nitrate anion (O6/O7/O8) and the DDOP alcohol group (O1). There are subtle differences between the networks, most importantly in the hydrogen bonds to the nitrate anion. In compound **1**, these are truly (although asymmetrically) bifurcated with H...A

distances of 2.21(2)–2.34(3) Å for O1...O6–O8 and 2.09(2)–2.27(2) Å for O2...O7–O8. In **2** and **3** the asymmetry of these “bifurcated” hydrogen bonds is more pronounced, with large differences between the H...A distances (of 0.37–0.6 Å) suggesting that they may be best viewed as two-centered hydrogen bonds (Table 3), considered to be stronger.¹⁷ In all three structures, hydrophobic C–H... π interactions help bring the layers together to form the crystal, as indicated by a number of short C...C contacts (*ca.* 3.36–3.92 Å).¹⁸

Co(II)–Cu(II) solid solutions (**4–6**)

$[\text{Co}_x\text{Cu}_{1-x}(\text{DDOP})(\text{NO}_3)(\text{H}_2\text{O})](\text{NO}_3)$ solid solutions (**4** to **6**) were synthesized in analogous fashion to monometallic compounds **1** to **3**, by using 1 : 1, 1 : 3 and 3 : 1 ratios of cobalt(II) and copper(II) nitrate. Respectively, these Co : Cu ratios resulted in the ICP-OES established compositions Co_{0.4}Cu_{0.6} (**4**), Co_{0.1}Cu_{0.9} (**5**) and Co_{0.7}Cu_{0.3} (**6**), indicating a preference for inclusion of the Cu-based complex cation. Only one metal site is observed crystallographically (Fig. 3 and S1†), indicating a disordered distribution of copper and cobalt sites in an overall structure of the type seen for **1** to **3** (Fig. 2). Although linear unit cell volume–composition correlations are seen in some solid solution coordination frameworks,¹⁹ no such relationship exists in **4** to **6**. The complex cations in **4** to **6** all have geometries intermediate between the Co and Cu analogues **1** and **2** (Table 2). Notably, in **4**, the axial bond lengths are significantly longer than those calculated by a 40 : 60 weighted average of the monometallic structures. The *average* axial elongations (over Co and Cu) of $\Delta(\text{M-OH}_2) = 0.030$ Å and $\Delta(\text{M-NO}_3) = 0.063$ Å in **4** are larger than the deviations (max. 0.024 Å) from calculated geometries in **5** and **6**, and are comparable to axial elongations induced in first row transition metals by intramolecular hydrogen bonds.⁴⁷ However, the high quality, positional disorder-free structure indicates minimal deviation of the two metals from the crystallographically observed geometry. Therefore most, or all, of the elongation in **4** must occur at the Co^{II} centres and the Cu–O distances may contract slightly compared to **2**. The resulting axial elongations of the Co–O bonds can be estimated at $\Delta(\text{Co-OH}_2) \approx 0.08$ Å and $\Delta(\text{Co-NO}_3) \approx 0.23$ Å when the Cu bond lengths of **2** are retained (see ESI†); and will be as high as $\Delta(\text{Co-OH}_2) = 0.170$ Å and $\Delta(\text{Co-NO}_3) = 0.281$ Å if Co^{II} and Cu^{II} both have

Table 3 Hydrogen bonding distances ($R/\text{\AA}$), angles ($\phi/^\circ$) and summed hydrogen bond valences ($\Sigma\text{Val}_{\text{H}\cdots\text{O}}$ /valence units) for **1–6**

Interaction		1	2	3	4	5	6
O1–H19...O6	$R_{\text{O}\cdots\text{O}}$	3.110(4)	2.873(2)	2.919(4)	2.903 (3)	2.875(3)	3.036(7)
	$R_{\text{H}\cdots\text{O}}$	2.21(2)	1.98(2)	2.00(2)	1.99(2)	1.99(2)	2.15(3)
	$\phi_{\text{O}\cdots\text{H}\cdots\text{O}}$	168(3)	173(3)	167(4)	171(3)	170(3)	157(4)
O1–H19...O8	$R_{\text{O}\cdots\text{O}}$	3.001(4)	3.220(3)	3.189(4)	3.184(3)	3.211(3)	3.067(7)
	$R_{\text{H}\cdots\text{O}}$	2.34(3)	2.58(2)	2.51(4)	2.51(3)	2.57(3)	2.30(4)
	$\phi_{\text{O}\cdots\text{H}\cdots\text{O}}$	129(2)	129(2)	129(3)	130(3)	129(2)	138(4)
O2–H1W...O7	$R_{\text{O}\cdots\text{O}}$	2.922(4)	3.242(3)	3.236(5)	3.210(4)	3.231(3)	3.040(8)
	$R_{\text{H}\cdots\text{O}}$	2.09(2)	2.47(2)	2.43(2)	2.40(2)	2.46(2)	2.25(5)
	$\phi_{\text{O}\cdots\text{H}\cdots\text{O}}$	152(2)	145(2)	145(3)	145(3)	143(3)	140(5)
O2–H1W...O8	$R_{\text{O}\cdots\text{O}}$	3.087(4)	2.917(2)	2.910(4)	2.947(3)	2.917(3)	3.064(6)
	$R_{\text{H}\cdots\text{O}}$	2.27(2)	2.08(2)	2.06(2)	2.08(2)	2.07(2)	2.15(3)
	$\phi_{\text{O}\cdots\text{H}\cdots\text{O}}$	150(2)	155(2)	152(3)	154(3)	156(3)	164(6)
O2–H2W...O5	$R_{\text{O}\cdots\text{O}}$	2.739(2)	2.786(2)	2.735(3)	2.763(3)	2.780(2)	2.742(5)
	$R_{\text{H}\cdots\text{O}}$	1.87(2)	1.93(2)	1.85(2)	1.87(2)	1.89(2)	1.87(3)
	$\phi_{\text{O}\cdots\text{H}\cdots\text{O}}$	160(3)	166(3)	164(4)	162(3)	168(3)	152(6)
$\Sigma\text{Val}_{\text{H}\cdots\text{O}}^a$	$R_{\text{O}\cdots\text{O}}$	0.467(2)	0.497(2)	0.508(3)	0.491(3)	0.499(2)	0.450(4)
	$R_{\text{H}\cdots\text{O}}$	0.51(2)	0.55(2)	0.58(2)	0.57(2)	0.56(2)	0.51(3)

^a Sum of the estimated bond valences for all hydrogen bonds per formula unit. Bifurcated hydrogen bonds are treated as a two-center interaction, basing $\text{Val}_{\text{H}\cdots\text{O}}$ on the shorter $R_{\text{H}\cdots\text{O}}$.²² Bond valences are calculated using ref. 20a ($R_{\text{O}\cdots\text{O}}$) and ref. 20b ($R_{\text{H}\cdots\text{O}}$). Errors on $\Sigma\text{Val}_{\text{H}\cdots\text{O}}$ are the sum of errors on contributing $\text{Val}_{\text{H}\cdots\text{O}}$ values, resulting from crystallographic ESDs.

exactly the crystallographically observed geometry. Such axial elongation of Co is supported by magnetic susceptibility data consistent with tetragonally distorted Co^{II} (see below).

The axial elongation of Co^{II} in **4** is larger than in previous examples induced by intramolecular hydrogen bonding.^{4f} The isostructural nature of the complex cations in **1–6**, and their near isomorphous crystal packing, means that their hydrogen bonded networks can usefully be examined to find a driving force for this distortion of Co^{II} . These networks are likely to be involved in the distortion as in their absence it is probable that the geometry mismatch between Co^{II} and Cu^{II} would prevent crystallization of the observed solid solutions, and separate monometallic solid phases would be expected. Logically, it is expected that **3** should adopt the most stable hydrogen bonded network, as Zn^{II} ($3d^{10}$) has poorly defined metal coordination preferences and should best allow the network to maximize the strength of its hydrogen-bonding interactions. The distances and angles observed in the hydrogen bonded network of **4** and **5** ($\text{Co}_{0.1}\text{Cu}_{0.9}$) are more similar to Zn-based **3** (and Cu-based **2**) than the Co compound **1** (Table 3), suggesting that stabilization of the crystal lattice through the strongest hydrogen bonded network overcomes the coordination preferences of Co^{II} . Such stabilization is also consistent with the apparent preference for inclusion of the Cu-based complex cation.

Bond valence estimation of hydrogen bonded network stability

The hypothesis that the hydrogen-bonded network of **4** distorts Co^{II} is supported by analysis of the relative strength of the hydrogen bonding interactions. For this we use the bond valence model^{16,20} as a simple, empirical alternative to theoretical methods such as DFT.^{7c} Bond valence calculations are frequently and accurately used to assess the relative contribution of hydrogen bonding in mineral structures,^{20b,21} and have also been used to evaluate molecular dynamics calculations on the structure of liquid water.²² Importantly, the valence–distance correlations^{16,20}

are well-established for the $\text{O–H}\cdots\text{O}$ hydrogen bonds discussed here.

Summed bond valences ($\Sigma\text{Val}_{\text{H}\cdots\text{O}}$) of the hydrogen bonds in **1–6** are presented in Table 3. While errors in $\Sigma\text{Val}_{\text{H}\cdots\text{O}}$ based on $\text{H}\cdots\text{O}$ distances are relatively large, the $\text{O}\cdots\text{O}$ based $\Sigma\text{Val}_{\text{H}\cdots\text{O}}$ values are precise and provide a reasonable basis for comparison due to the minimal variation in $\text{O–H}\cdots\text{O}$ angles between the structures. The $\Sigma\text{Val}_{\text{H}\cdots\text{O}}$ values for both methods indicate that, as expected, **3** has the most stable hydrogen bonded network, and of the monometallic solids Co compound **1** has the least stable. The $\Sigma\text{Val}_{\text{H}\cdots\text{O}}$ values of **2**, **4** and **5** are essentially the same within experimental error, and only slightly lower than for **3** (by *ca.* 0.01 to 0.03 valence units). Solid solution **6** ($\text{Co}_{0.7}\text{Cu}_{0.3}$) has a similar or slightly lower $\Sigma\text{Val}_{\text{H}\cdots\text{O}}$ to **1**.

The drop in $\Sigma\text{Val}_{\text{H}\cdots\text{O}}$ of 0.04 ($\text{O}\cdots\text{O}$ -based) to 0.07 v.u. ($\text{H}\cdots\text{O}$ -based) between **3** and **1** (and **6**) is significant, especially considering that the two-center treatment of the more truly bifurcated hydrogen bonds in **1** and **6** is likely to overestimate $\Sigma\text{Val}_{\text{H}\cdots\text{O}}$ for these structures.^{‡17} Assuming a typical O–H bond dissociation energy of around 450 kJ mol^{-1} ,²³ the tabulated values of $\Sigma\text{Val}_{\text{H}\cdots\text{O}}$ imply destabilization of **1** and **6** by 14–18 kJ mol^{-1} relative to **2**, 18–32 kJ mol^{-1} relative to **3**, and 11–27 kJ mol^{-1} relative to **4**: that is, by approximately the energy of one $\text{O–H}\cdots\text{O}$ hydrogen bond²⁴ per formula unit compared to the other networks. It can therefore be seen that subtle changes in a hydrogen bonded network can exert just as effective distorting forces on a metal center as intramolecular hydrogen bonding. In solid solution **4** the Co^{II} geometry elongates, as a mismatch between the Cu^{II} and Co^{II} geometries shifts the balance between optimising the Co^{II} coordination sphere and the stability of the

‡ The pronounced asymmetry of the “bifurcated” hydrogen bonds in **2** to **4** means that it is reasonable to treat them as two-center interactions. In the case of **1**, bifurcated hydrogen bonds are considered to be weaker than two-center hydrogen bonds, so the two-center approach applied here is likely to have overestimated the total bond valence. For a theoretical treatment of bifurcated hydrogen bonds see ref. 17.

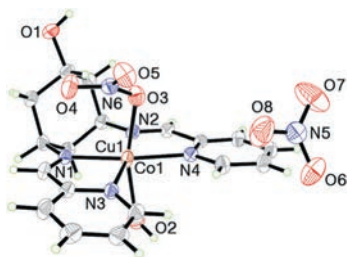


Fig. 3 Crystal structure of the solid solution **4**. ADP ellipsoids are drawn at 50% probability level. Color scheme as Fig. 1 with Co–Cu brown; Cu and Co atoms are disordered over the same site.

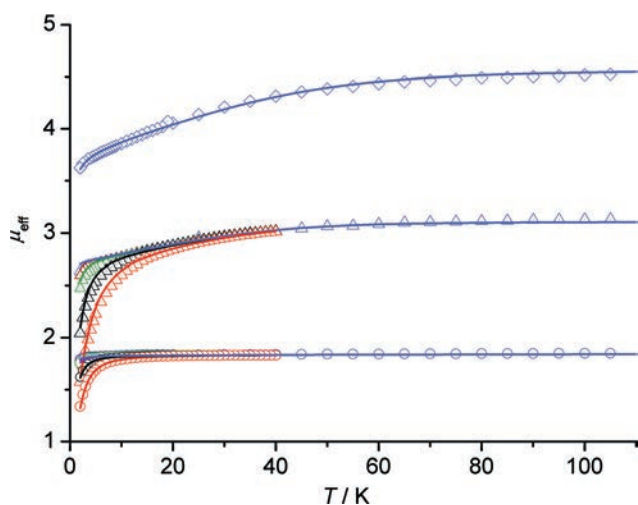


Fig. 4 Temperature dependence of μ_{eff} for **1** (diamonds), **2** (circles) and **4** (triangles) at static fields of 0.1 (blue), 0.5 (purple), 1.0 (green), and 5.0 (red) Tesla.

hydrogen bonded network. In solid solution **6**, however, the dominant presence of Co^{II} (70%) is able to overcome the preference of the network for axial elongation and possibly impose an axial contraction on Cu^{II} .

While approximate, the figures above show the potential of the bond valence approach as a simple aid to understanding the contribution of hydrogen bonding in molecular structures. Precision could be substantially improved in structures with accurately located H atoms; e.g. neutron diffraction data.

Magnetic properties of compounds **1**, **2** and **4**

Variable temperature magnetic susceptibility measurements were performed on **1**, **2** and **4** in the range of 2 to 290 K, with a variety of magnetic field strengths (Fig. 4 and Table 4). Previous studies of magnetic coupling through hydrogen bonds have focused on relatively short metal–metal separations through M–OH...O–M linkages, often featuring multiple hydrogen bonds. These can give rise to both ferro-⁵ and, usually, antiferromagnetic couplings^{5a,c,6} with small exchange energies (J), although examples of strong antiferromagnetic interactions are known with J of up to -90 cm^{-1} .^{6a-d} The M–OH...ONO₂–M connections in **1–3** are longer and expected to give only weak couplings.

Table 4 Parameters for the magnetic analysis of **1**, **2** and **4**

Compound	1	2	4
$3d^N$	d^7	d^9	d^7/d^9
B/cm^{-1} ($C = 4B$)	825	—	1115/960
ζ/cm^{-1}	533	829	380/347
$C/10^{-6} \text{ m}^3 \text{ K mol}^{-1}$	—	5.320	—
$\mu_{\text{eff}}(290 \text{ K})$	4.54	1.84	3.12
$B_0^2/10^4 \text{ cm}^{-1}$	0.52	—	0.457
$B_0^4/10^4 \text{ cm}^{-1a}$	3.35	5.80	3.11
B_4^4/B_0^4	0.58	0.6	0.45
Co : Cu ratio ($1 - \alpha : \alpha$)	—	—	0.41 : 0.59
$\lambda_{\text{mf}}/10^5 \text{ mol m}^{-3}$	-1.1	-0.17	-1.48
θ/K	—	-0.09	—
SQ^b	0.6%	0.4%	0.9%

^a $Dq = B_0^4/21 = 1595 \text{ cm}^{-1}$ (**1**); 2760 cm^{-1} (**2**); 1485 cm^{-1} (**4**).

^b Goodness of fit is quantified as $SQ = (FQ)^{1/2}$ where $FQ = \sum_{i=1}^n (\chi_{\text{obs}}(i) - \chi_{\text{cal}}(i))/\chi_{\text{obs}}(i)^2$.

The magnetochemical analysis of Co^{II} -based complexes **1** and **4** requires consideration of a multitude of factors, notably the fact that the Co^{II} free-ion 4F ground term is separated by the first excited state 4P by ca. 10^4 cm^{-1} .²⁵ In a weak octahedral ligand field, the 4F term splits into $^4T_1(F)$, 4T_2 , and 4A_2 terms, while the 4P term transforms into a $^4T_1(P)$ term. The magnetic properties of Co^{II} ($3d^7$) octahedral high-spin complex thus imply a significant temperature dependence of μ_{eff} (or χT) caused by orbital momentum contributions according to the triplet ground state $^4T_1(F)$. On the other hand, octahedral high-spin complexes of Cu^{II} with an orbital doublet ground state (2E) represent near-ideal pure spin systems,²⁶ though axial Jahn–Teller elongation confines the magnetic 3d orbital to the equatorial plane.

For compounds **1** and **4** the following single-ion effects were evaluated: interelectronic repulsion (H_{ee}), spin–orbit coupling (H_{so}), ligand–field effect (H_{lf}), and the applied field (H_{mag}) employing the effective Hamiltonian:

$$\hat{H} = \underbrace{\sum_{i=1}^N \left[-\frac{\hbar^2}{2m_e} \nabla_i^2 + V(r_i) \right]}_{\hat{H}^{(0)}} + \underbrace{\sum_{i>j}^N \frac{e^2}{r_{ij}}}_{\hat{H}_{\text{ee}}} + \underbrace{\sum_{i=1}^N \zeta(r_i) \kappa \hat{\mathbf{l}}_i \cdot \hat{\mathbf{s}}_i}_{\hat{H}_{\text{so}}} + \underbrace{\sum_{i=1}^N \sum_{k=0}^{\infty} \left\{ B_0^k C_0^k(i) + \sum_{q=0}^k \left[B_q^k (C_{-q}^k(i) + (-1)^q C_q^k(i)) \right] \right\}}_{\hat{H}_{\text{lf}}} + \underbrace{\sum_{i=1}^N \mu_B (\kappa \hat{\mathbf{l}}_i + 2\hat{\mathbf{s}}_i) \cdot \mathbf{B}}_{\hat{H}_{\text{mag}}}$$

While $H^{(0)}$ represents the energy in the central field approximation, H_{ee} and H_{so} account for interelectronic repulsion and spin–orbit coupling (modified by the orbital reduction factor κ), respectively. The former is taken into account by the Racah parameters B and C , the latter by the one-electron spin–orbit coupling parameter ζ . These sets of interelectronic repulsion parameters and ζ are used as constants in the fitting procedure. H_{lf} accounts for the electrostatic effect of the ligands in the framework of ligand field theory on the basis of the global parameters B_q^k . The spherical tensors C_q^k are directly related to the

spherical harmonics $B_q^k = \sqrt{4\pi/(2k+1)}Y_q^k$ and the real ligand field parameters B_q^k (Wybourne notation,²⁷ see ref. 28 for relations between the parameters B_q^k and Dq , Ds , Dt , etc. for cubic, tetragonal, etc. systems) are given by $A_q^k \langle r^k \rangle$ where A_q^k represents a numerical constant describing the charge distribution in the environment of the metal ion and $\langle r^k \rangle$ is the radial wave function expectation value. For d electrons the terms in the expansion with $k \leq 4$ are non-zero, and all odd- k terms vanish. The values of k and q are limited by the point symmetry of the metal ion site. Note that in cubic systems only spherical tensors with $k \leq 4$ are relevant. For a tetragonal ligand field, the ligand field operator with reference to the fourfold rotation axis for the angular part of the wave function reads

$$H_{\text{lf}}^{\text{tr}} = B_0^2 \sum_{i=1}^N C_0^2(i) + B_0^4 \sum_{i=1}^N C_0^4(i) + B_4^4 \sum_{i=1}^N (C_4^4(i) + C_{-4}^4(i))$$

Note, for cubic systems a fixed relationship exists between $B_4^4 = \sqrt{5/14}B_0^4$. The matrix elements of H , omitting $H^{(0)}$, are evaluated by applying $H = H_{\text{lf}} + H_{\text{ee}} + H_{\text{so}} + H_{\text{ex}} + H_{\text{mag}}$ on the full basis of microstates (120 and 10 functions for Co^{2+} and Cu^{2+} , respectively). Any residual inter-complex coupling is accounted for by molecular field approximation:

$$\chi_{\text{m}}^{-1} = \chi_{\text{m}}'^{-1}(B, C, \zeta, B_q^k, B_0) - \lambda_{\text{mf}}$$

The temperature-dependent susceptibility measurements of polycrystalline samples of **1**, **2** and **4** are shown in Fig. 4 as μ_{eff} vs. T . Note that for **2** μ_{eff} is temperature independent at $T > 20$ K whereas a significant decrease of μ_{eff} is observed for **1** and **4** below 100 K.

Magnetochemical analysis of the Cu(II) complex 2

For compound **2** Curie–Weiss behavior $\chi_{\text{m}} = C/(T-\theta)$ is observed, with $C = 5.32 \times 10^{-6} \text{ cm}^3 \text{ K mol}^{-1}$ corresponding to $\mu = 1.84 \mu_{\text{B}}$ and a small value for $\theta = -0.09$ K, indicating only small deviations from a perfect Curie paramagnet. The combined effect of a weak antiferromagnetic Cu...Cu interaction and magnetic saturation are responsible for the decrease of μ_{eff} below 20 K. Note that these intermolecular interactions can also be modeled for $\lambda_{\text{mf}} = -1.7 \times 10^4 \text{ m}^3 \text{ mol}^{-1}$, corresponding to $\theta = -0.09$ K in the case of a pure spin system ($\theta = C\lambda_{\text{mf}}$). As is common for Jahn–Teller distorted Cu(II) centers, μ is increased from its spin-only value of $1.73 \mu_{\text{B}}$ ($3d^9$, E ground term) due to its positive spin–orbit coupling constant λ_{LS} ($\zeta = \pm 2S/\lambda_{\text{LS}}$).

Magnetochemical analysis of the Co(II) complex 1

The effective magnetic moment of the cobalt complex **1** at 290 K is 4.72 per Co(II) ion, slightly smaller than the value resulting for both spin and orbital momentum, $\mu_{\text{LS}} = [L(L+1) + 4S(S+1)]^{1/2} = 5.20 \mu_{\text{B}}$. For octahedral Co(II) high-spin complexes ($S = 3/2$) in magnetically dilute systems, μ_{eff} values in the range 4–5 are expected as a result of spin and first-order orbital contributions. To assess the ligand–field effect, spin–orbit coupling, and exchange coupling has been taken into account. The values for the spin–orbit coupling energy and the Racah parameter were listed in Table 1 and based on standard UV/VIS data.²⁹

The parameters λ_{mf} and B_0^4 are fitted to the low-field susceptibility data to yield $\lambda_{\text{mf}} = -1.1 \times 10^4 \text{ mol m}^{-3}$ and $B_0^4 = 33500 \text{ cm}^{-1}$ ($Dq = B_0^4/21 = 1595 \text{ cm}^{-1}$). The small molecular parameter indicates a weak antiferromagnetic interaction between the magnetic centers, and the decrease of μ_{eff} towards low temperatures is primarily caused by single ion effects.

Magnetochemical analysis of the mixed-metal compound 4

The mixed compound **4** was evaluated first by direct comparison to the susceptibility of **1** and **2**

$$\chi_{\text{m}}(\mathbf{4}) = \alpha\chi_{\text{m}}(\mathbf{1}) + (1 - \alpha)\chi_{\text{m}}(\mathbf{2})$$

to describe its metal constituent ratio $\text{Co}_{\alpha}\text{Cu}_{1-\alpha}$.³⁰ The high-temperature value of μ_{eff} is lower than the estimated value for an initially presumed 50 : 50 ($\mu_{\text{eff}} = 3.46$) composition of the pure components **1** and **2**; from the room-temperature susceptibilities, a ratio Co : Cu \approx 2 : 3 was estimated. To calculate the complete susceptibility data set of **4** by varying x in addition to the parameter set B_0^2 , B_0^4 , B_4^4/B_0^4 , and λ_{mf} proved unsuccessful because of parameter correlation and overparameterization.

Thus, we modeled the magnetic susceptibility data of **4** based on combined field- and temperature-dependent data. This enabled refinement of the Co : Cu ratio, where the cubic components of the Co(II) ligand field were fixed, namely at $B_0^4 = 31100 \text{ cm}^{-1}$ and $B_4^4/B_0^4 = 0.45$. This considerably lower value – compared to the cubic values for compound **1** – directly reflects the changes to the Co(II) ligand field caused by the solid solution network mismatch in **4**, i.e. the elongation of the M–O and M–N (M = Co and Cu) mean distance in **4** compared to **1** (see Table 2). A least-squares fit (Fig. 4) results in $\alpha = 0.59$, i.e. to the mixed-metal composition $\text{Co}_{0.41}\text{Cu}_{0.59}$. For **4** the parameter values B_0^2 and λ_{mf} are reduced compared to those in **1**, indicating that the tetragonal distortion as well as the interatomic exchange interactions of antiferromagnetic nature in **4** are weaker than in **1** and **2**.

Conclusions

Co-crystallization of isostructural Co(II) and Cu(II) complexes forces axial elongation on the cobalt centers to fit in with the Cu(II)-based network, assisted by the more stable hydrogen bonded network associated with the Cu(II) compound; as indicated by bond-valence calculations. Larger loadings of cobalt (70%) are able to overcome this network preference, demonstrating a fine balance between optimal metal coordination geometry and the most stable hydrogen bonded network. Bond valence calculations also demonstrate that the cumulative effect of small changes to a hydrogen bonded network may equal the effect of an additional hydrogen bond, a result indicating the potential utility of bond-valence calculations as a simple method for analysis of hydrogen bonding in molecular as well as mineral structures. Additionally, the influence of the altered Co(II) geometry on the observed magnetic properties opens perspectives for hydrogen-bonded solid solutions as a means of modulating the solid state magnetic and optical properties of metal complexes.

Acknowledgements

We thank Claire Besson for suggesting use of the bond-valence method, Georg Seeber for X-ray diffraction data for compound **2**, Kevin Lamberts for X-ray diffraction data on the additional solid solutions (ESI) and Geoff Cooper for re-synthesis of **4**. JF and DL both acknowledge the EPSRC for funding.

Notes and references

- (a) H. W. Roesky and M. Andruh, *Coord. Chem. Rev.*, 2003, **236**, 91; (b) B. Moulton and M. J. Zaworotko, *Chem. Rev.*, 2001, **101**, 1629; (c) D. G. Braga, L. Brammer and N. R. Champness, *CrystEngComm*, 2005, **7**, 1; (d) M. D. Ward, *Chem. Commun.*, 2005, 5838; (e) J. D. Wuest, *Chem. Commun.*, 2005, 5830; (f) R. J. Hill, D.-L. Long, N. R. Champness, P. Hubberstey and M. Schröder, *Acc. Chem. Res.*, 2005, **38**, 337.
- (a) A. Nangia, *Acc. Chem. Res.*, 2008, **41**, 595; (b) K. Fucke, N. Qureshi, D. S. Yufit, J. A. K. Howard and J. W. Steed, *Cryst. Growth Des.*, 2010, **10**, 880.
- S. Liu and B. C. Gibb, *Chem. Commun.*, 2008, 3709.
- (a) K. Johnson and J. W. Steed, *J. Chem. Soc., Dalton Trans.*, 1998, 2601; (b) D. Braga, F. Grepioni and G. R. Desiraju, *Chem. Rev.*, 1998, **98**, 1375; (c) J. W. Steed and P. C. Junk, *J. Chem. Soc., Dalton Trans.*, 1999, 2141; (d) J. W. Steed, B. J. McCool and P. C. Junk, *J. Chem. Soc., Dalton Trans.*, 1998, 3417; (e) J. W. Steed, K. Johnson, C. Legido and P. C. Junk, *Polyhedron*, 2003, **22**, 769; (f) D. R. Turner, M. B. Hursthouse, M. E. Light and J. W. Steed, *Chem. Commun.*, 2004, 1354; (g) J. Fielden, D.-L. Long and L. Cronin, *Chem. Commun.*, 2004, 2156; (h) J. Fielden, P. T. Gunning, D.-L. Long, M. Nutley, A. Ellern, P. Kögerler and L. Cronin, *Polyhedron*, 2006, **25**, 3474.
- (a) M. S. Ray, A. Ghosh, R. Bhattacharya, G. Mukhopadhyay, M. G. B. Drew and J. Ribas, *Dalton Trans.*, 2004, 252; (b) Y. Ma, A.-L. Cheng and E.-Q. Gao, *Dalton Trans.*, 2010, **39**, 3521; (c) G. Nieuwpoort, G. C. Verschoor and J. Reedijk, *J. Chem. Soc., Dalton Trans.*, 1983, 531; (d) M. Ardon, A. Bino, K. Michelsen and E. Pedersen, *J. Am. Chem. Soc.*, 1987, **109**, 5855.
- Selected examples: (a) J. A. Bertrand, T. D. Black, P. G. Eller, F. T. Helm and R. Mahmood, *Inorg. Chem.*, 1976, **15**, 2965; (b) J. A. Bertrand, E. Fujita and D. G. Vanderveer, *Inorg. Chem.*, 1980, **19**, 2022; (c) H. Muhonen, *Inorg. Chem.*, 1986, **25**, 4692; (d) J. Tang, J. S. Costa, A. Golobič, B. Kozlevčar, A. Robertazzi, A. V. Vargiu, P. Gamez and J. Reedijk, *Inorg. Chem.*, 2009, **48**, 5473; (e) U. Bossek, K. Wiegardt, B. Nuber and J. Weiss, *Angew. Chem., Int. Ed. Engl.*, 1990, **29**, 1055; (f) T. K. Paine, T. Weyhermüller, K. Wiegardt and P. Chaudhuri, *Inorg. Chem.*, 2002, **41**, 6358; (g) M. S. Ray, A. Ghosh, S. Chaudhuri, M. G. B. Drew and J. Ribas, *Eur. J. Inorg. Chem.*, 2004, 3110.
- Selected examples: (a) G. R. Lewis and A. G. Orpen, *Chem. Commun.*, 1998, 1873; (b) K. A. Siddiqui, G. K. Mehrotra and R. L. LaDuca, *Polyhedron*, 2009, **28**, 4077; (c) S. R. Choudhury, B. Dey, S. Das, A. Robertazzi, A. D. Jana, C.-Y. Chen, H. M. Lee, P. Gamez and S. Mukhopadhyay, *Dalton Trans.*, 2009, 7617.
- (a) J. Fielden, J. Sprott and L. Cronin, *New J. Chem.*, 2005, **29**, 1152; (b) J. Fielden, J. Sprott, D.-L. Long, P. Kögerler and L. Cronin, *Inorg. Chem.*, 2006, **45**, 2886; (c) J. Fielden, D.-L. Long, A. M. Z. Slawin, P. Kögerler and L. Cronin, *Inorg. Chem.*, 2007, **46**, 9090.
- (a) J. Fielden, D.-L. Long, C. Evans and L. Cronin, *Eur. J. Inorg. Chem.*, 2006, 3930; (b) J. Fielden, *PhD thesis*, University of Glasgow, Glasgow, 2004.
- M. Speldrich, H. Schilder, H. Lueken and P. Kögerler, *Isr. J. Chem.*, 2011, **51**, 215.
- G. M. Sheldrick, *Acta Crystallogr.*, 1990, **A46**, 467.
- Programs for Crystal Structure Analysis (Release 97-2), Institut für Anorganische Chemie der Universität Göttingen, Göttingen, Germany, 1998.
- L. J. Farrugia, *J. Appl. Crystallogr.*, 1999, **32**, 837.
- SHELXTL (Version 6.12), Bruker AXS Inc, Madison, Wisconsin, USA, 2001.
- R. H. Blessing, *Acta Crystallogr., Sect. A: Found. Crystallogr.*, 1995, **A51**, 33.
- I. D. Brown and D. Altermatt, *Acta Crystallogr., Sect. B: Struct. Sci.*, 1985, **B41**, 244.
- I. Rozas, I. Alkorta and J. Elguero, *J. Phys. Chem. A*, 1998, **102**, 9925.
- C. Janiak, *J. Chem. Soc., Dalton Trans.*, 2000, 3885.
- M.-H. Zeng, B. Wang, X.-Y. Wang, W.-X. Zhang, X.-M. Chen and S. Gao, *Inorg. Chem.*, 2006, **45**, 7069.
- (a) G. Ferraris and G. Ivaldi, *Acta Crystallogr., Sect. B: Struct. Sci.*, 1988, **B44**, 341; (b) I. D. Brown, *The Chemical Bond in Inorganic Chemistry: The Bond Valence Model*, Oxford University Press, New York, USA, 2002.
- For recent examples see: (a) A. R. Kampf, G. R. Rossman and R. M. Housley, *Am. Mineral.*, 2009, **94**, 1198; (b) M. Nagashima, M. Akasaka, T. Minakawa, E. Libowitzky and T. Armbruster, *Am. Mineral.*, 2009, **94**, 1440; (c) P. Elliott, G. Giester, E. Libowitzky and U. Kolitsch, *Am. Mineral.*, 2010, **95**, 397.
- B. R. Bickmore, K. M. Rosso, I. D. Brown and S. Kerisit, *J. Phys. Chem. A*, 2009, **113**, 1847.
- CRC Handbook of Chemistry and Physics*, ed. W. M. Haynes and D. R. Lide, CRC Press, Boca Raton, Florida, USA, 90th edn, 2009.
- G. A. Jeffrey, *An Introduction to Hydrogen Bonding (Topics in Physical Chemistry)*, Oxford University Press, New York, USA, 1997.
- (a) B. N. Figgis and M. A. Hitchman, *Ligand Field Theory and Its Applications*, Wiley-VCH, New York, 2000; (b) J. S. Griffith, *The Theory of Transition-Metal Ions*, Cambridge University Press, Cambridge, 1971.
- O. Kahn, *Molecular Magnetism*, VCH, Weinheim, 1993.
- (a) K. B. Gorller-Walrand, in *Handbook on the Physics and Chemistry of Rare Earths*, ed. K. A. Gschneidner and L. Eyring, Elsevier, Amsterdam, 1996, vol. 23, p. 121; (b) B. G. Wybourne, *Spectroscopic Properties of Rare Earths*, Wiley, New York, London, Sydney, 1965.
- (a) C. J. Ballhausen, *Ligand Field Theory*, McGraw-Hill, New York, 1962; (b) E. König and S. Kremer, *Magnetism Diagrams for Transition Metal Ions*, Plenum Press, New York, London, 1979.
- A. B. P. Lever, *Inorganic Electronic Spectroscopy*, Elsevier, Amsterdam, 1984.
- For a similar fitting approach see: M.-D. Serb, M. Speldrich, H. Lueken and U. Englert, *Z. Anorg. Allg. Chem.*, 2011, **637**, 536.